Hindawi Publishing Corporation
Active and Passive Electronic Components
Volume 2012, Article ID 652478, 12 pages
doi:10.1155/2012/652478

Research Article

A Unified Channel Charges Expression for Analytic MOSFET Modeling

Hugues Murray and Patrick Martin

Normandie Université, Ensicaen, UMR 6508, LaMIPS, Laboratoire Commun CNRS-NXP-PRESTO-ENSICAEN UCBN, 6 boulevard Maréchal Juin, 14050 CAEN Cedex 4, France

Correspondence should be addressed to Hugues Murray, hugues_murray@presto-eng.com

Received 22 June 2012; Accepted 9 November 2012

Academic Editor: Gerard Ghibaudo

Based on a 1D Poissons equation resolution, we present an analytic model of inversion charges allowing calculation of the drain current and transconductance in the Metal Oxide Semiconductor Field Effect Transistor. The drain current and transconductance are described by analytical functions including mobility corrections and short channel effects (CLM, DIBL). The comparison with the Pao-Sah integral shows excellent accuracy of the model in all inversion modes from strong to weak inversion in submicronics MOSFET. All calculations are encoded with a simple C program and give instantaneous results that provide an efficient tool for microelectronics users.

1. Introduction

Although MOSFET modeling is now well covered and addressed in BSIM, EKV, and PSP compact models [1], it is always interesting to present a semianalytic resolution of 1D Poissons equation which can be implemented in popular computers with usual software giving most physical results (potential and charges distribution) instantaneously. New approaches of MOSFET surface potential modeling were performed from analytic treatment and have brought a renewal in analytic resolution of surface potential [2–5]. We previously used a similar method in the analytic description of surface potential by Taylor expansion [6].

Oguey and Cserveny [7] proposed as early as 1982 a complete analytic model based on the gate and drain source voltages. An important step was reached in modeling by Enz et al. in 1995 [8], Iniguez et al. [9] in 1996, and Cheng [10] in 1998 who gave analytic expression of the inversion charge. We certainly do not pretend to provide an alternative method to the compact models implemented on the simulators for CAD, but are simply trying to provide analytical support to the understanding of strategic components of microelectronics.

From the analytical expression of inversion charge as a function of gate and drain bias, we attempted to provide a single analytical expression that achieves explicit functions of the drain current $I_D\ (Vg, V_D)$ and the transconductance $g(Vg, V_D)$. The originality is based on a model in which the threshold voltage does not appears explicitly, but is replaced in the analytical expression by a parameter $b(Vg)$ dependent on the surface potential at zero drain bias.

It became obvious to us that the influence of other parameters could be included in these equations by more complex developments based on quasi two-dimensional analysis that exceeded this paper. Thus, we have not considered the specific effects: ballistic transport, tunneling through the oxide gate, which alone account for modeling of complex developments and led to numerical 2D treatments.

The presentation is made under the Gradual Channel Approximation (GCA) [11] which assumes that the electric field in the direction perpendicular to the channel is much greater than in the direction parallel to the channel and allows a 1D model of Poisson-Boltzmann equation. The different explicit equations (gate voltage and channel potential versus surface potential) are inverted using Taylor expansion, and we solve all equations until the point analytic

calculations can be done then calculate the single integrals by Simpson algorithm encoded in simple C programs.

2. Basic Assumptions in MOSFET

2.1. The Surface Potential Equation. Under the gradual channel approximation [11], with the introduction of the reduced channel voltage $\xi(y) = V(y)/U_T$ as quasi-Fermi potential [12] and the correct charges densities are [4]

$$\begin{aligned} n(x,y) &= n_i e^{u(x,y)-\xi(y)}, \\ p(x,y) &= p_i e^{-u(x,y)}, \\ N_A &= p_i e^{-u_b}, \\ N_D &= n_i e^{u_b-\xi(y)}. \end{aligned} \tag{1}$$

The Poisson-Boltzmann equation can be analytically solved using the 1Dmodel of Nicollian and Brews [13] from the charge density:

$$\frac{dF(x)}{dx} = \frac{q}{\varepsilon_S}[p(x,y) - n(x,y) + N_D - N_A]. \tag{2}$$

The surface electric field, $F_S(y) = F_x(0,y)$, along y (Figure 1) solution of (2) in $x = 0$, is

$$F_S(y) = \sqrt{\frac{2KTn_i}{\varepsilon_S}}\sqrt{e^{-\xi(y)}H[u_S(y)] + G[u_S(y)]}, \tag{3}$$

by setting:

$$\begin{aligned} H(u) &= e^u + e^{u_b}[u_b - u - 1], \\ G(u) &= e^{-u} - e^{-u_b}[u_b - u + 1]. \end{aligned} \tag{4}$$

The gate voltage Vg relative to flat band is

$$\begin{aligned} Vg - V_{\text{fb}} &= -\frac{Q_S(y)}{C_0} \\ &+ \Psi_S(y) = \gamma_0\sqrt{e^{-\xi(y)}H[u_S(y)] + G[u_S(y)]} \\ &+ U_T[u_S(y) - u(b)]. \end{aligned} \tag{5}$$

2.2. The Surface Potential Dependence to Gate and Drain Bias. The gate voltage is an explicit function of $u_S(y)$ and $\xi(y)$. Several solutions of $Vg = f[u_S(y), \xi(y)]$ were reported to express the band bending $\Psi_S = U_T[u_S(y) - u_b]$ as an analytic function of the gate and channel voltages [3, 14]. Gildenblat et al. have given in [5, 14] a noniterative expression of the surface potential which serves as a reference for surface potential-based models. In the following, we generated $u_S(y)$ by first-order Taylor expansion as previously done in [6].

$u_S(y)$ versus Vg at a constant drain bias $V(y)$ is generated by

$$u_S(l+1) = u_S(l) + \delta\left(\frac{du_s}{dVg}\right)_{u_s[l]}, \tag{6}$$

$Vg(l) = l \cdot \delta$, (δ sample step and l integer).

And $u_S(y) = u_{S,m}$ *versus* $V(y)$ at a constant Vg is generated by:

$$u_{S,m+1} = u_{S,m} + h\left[\frac{du_S}{d\xi}\right]_{u_S = u_{S,m}}. \tag{7}$$

$\xi(y) = mh$ (h sample step and m integer) is expressed as a function of $u_S(y)$ at a constant Vg by an analytic model previously developed by Baccarani et al. [15]:

$$\xi(y) = \ln\frac{H[u_S(y)]}{E[u_S(y)] - G[u_S(y)]} \tag{8}$$

with the introduction of the dimensionless quantity:

$$E(u) = \left[\frac{Vg - U_T(u - u_b)}{\gamma_0}\right]^2. \tag{9}$$

3. Analytic Model of Inversion Charges

3.1. The Inversion Charges Dependence to Gate and Drain Bias. In an n-MOSFET, the inversion charges are defined by the integral of electrons density over the "physical" thickness d_{inv}:

$$Q_{\text{inv}} = q\int_0^{d_i} n(x,y)\,dx. \tag{10}$$

The "physical" inversion starts at the silicon surface with the surface potential $u(0,y) = u_S(y)$ and ends at the abscissa $x = d_{\text{inv}}$ corresponding to $n(x,y) = p(x,y)$ and $u(d_{\text{inv}}, y) = \xi(y)/2$. The inversion charge dependence with channel potential $\xi(y)$ at a constant Vg noted $Q_{\text{inv}}(\xi(y))|_{V(g)}$ can be written in terms of potential as follows:

$$Q_{\text{inv}}(\xi(y))\,|_{V(g)} = \lambda q n_i \int_{\xi(y)/2}^{u(s)} \frac{e^{u-\xi(y)}du}{\sqrt{e^{-\xi(y)}H(u) + G(u)}}. \tag{11}$$

From (8), $Q_{\text{inv}}(\xi(y))|_{V(g)}$ becomes a single integral of u with the limits only dependent of m. Figure 2 shows $Q_{\text{inv}}(V(y))|_{V(g)}$ versus $V(y) = \xi(y) \cdot U_T$ with Vg as a parameter in linear (strong inversion) and log scale (weak inversion).

A threshold voltage of inversion charges $V_{DT}|_{V(g)}$ can be defined by the interpolation of the linear part of $Q_{\text{inv}}(V_D)|_{V(g)}$ with the V_D axis. $V_{DT}|_{V(g)} = f(Vg)$ plots (Figure 3) give at $V_D = 0$ a threshold voltage V_T which differs from V_{T0} by a factor ≈ 1.1. V_T is used in (12) instead of V_{T0}.

3.2. Analytic Expression of the Inversion Charges Dependence to Gate and Drain Bias. The simplest analytic approximate expression of $Q_{\text{inv}}(Vg, V_D)$ in the whole range of gate and drain bias is well represented by

$$Q_{\text{inv}}(Vg, V_D) = \eta C_0 U_T \ln\left[1 + \exp\left(\frac{Vg - V_T}{\eta_0 U_T} - \frac{V_D}{U_T}\right)\right]. \tag{12}$$

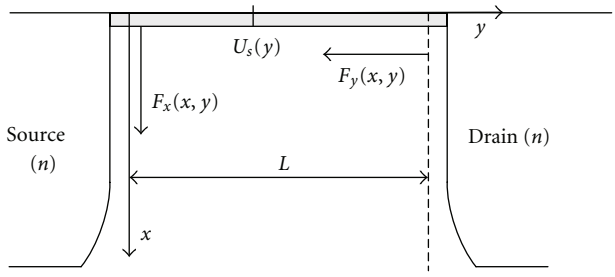

Figure 1: The n-MOSFET.

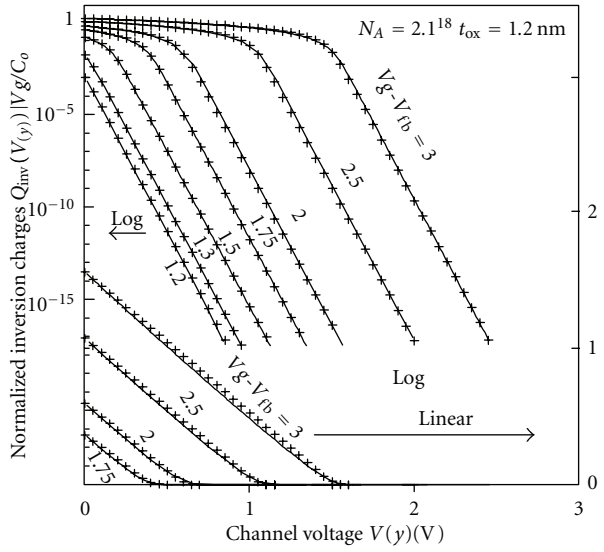

Figure 2: Normalized $[Q_{inv}(V(y))|_{Vg}, V(y)]$ plots in logarithm and linear scales. (−) (11), (+) (17).

$\eta_0(\approx 1.2)$ is the slope factor defined by the exponential law $Q_{inv}(Vg, 0)$ if $Vg < V_{T0}$.

However, this formulation should contain adjustment coefficients to reduce the error between (11) and (12). This was done in 1996 by Iniguez et al. [9] with the introduction of adjustment coefficients based on the threshold voltage in an expression of inversion charges similar with (12).

We propose an alternative method by introducing a "charge linearization factor," $\eta = \eta(Vg)$ which fits the slope $dQ_{inv}(V_D)|_{V(g)}/dV$ in strong inversion, and a preexponential parameter $a(Vg)$ which fits (12) with (11) in $y = 0$:

$$\tilde{Q}_{inv\,0}(Vg, V_D) = \eta(Vg) C_0 U_T \ln\left[1 + a(Vg) \exp\left(\frac{Vg - V_T}{\eta_0 U_T} - \frac{V_D}{U_T}\right)\right]. \quad (13)$$

Another definition of the "charge linearization factor" $\eta(\Psi_S)$ was introduced by Sallese et al. [16] in strong inversion and gives results different from $\eta(Vg)$ as shown in Figure 4. $\eta(\Psi_S)(>1)$ increases when Vg decreases. The difference between $\eta(\Psi_S)$ and $\eta(Vg)$ results from $d\Psi_S/dV_D = du_S/d\xi$ which can be calculated from (5). $\eta(Vg)$ and $a(Vg)$ are

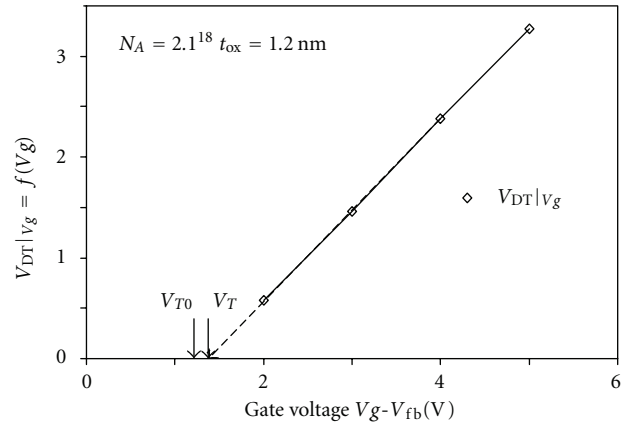

Figure 3: The threshold voltages $V_{DT}|_{V(g)} = f(Vg)$.

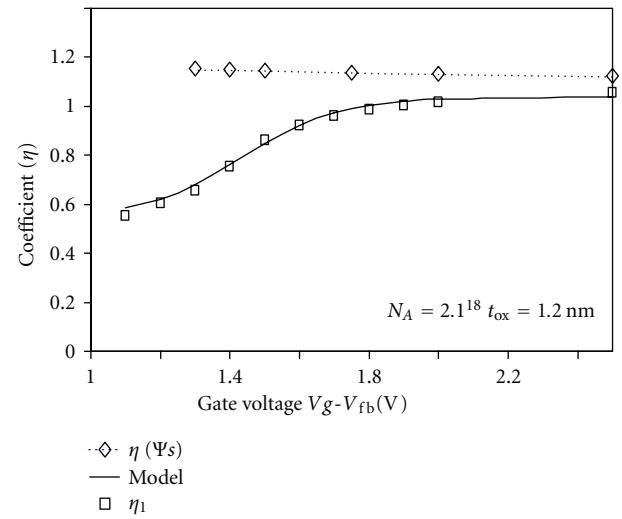

Figure 4: $\eta(Vg)$ modeling by exponential functions. ($\eta_{2f} = 1.08$; $N = 5.5$.)

interdependent and will be estimated in order to minimize the error between $Q_{inv}(V_D)|_{V(g)}$ and $\tilde{Q}_{inv\,0}(Vg, V_D)$.

Figure 4 shows $[\eta(Vg), Vg]$ plots calculated from $Q_{inv}(v(y))|_{V(g)}$ and $\eta(Vg)$ are well represented by a smoothing function η_{21}as follows:

$$\eta(Vg) \approx \eta_{21} = \frac{\eta_{2f}}{2} \frac{1 + \exp((Vg - V_{T0})/NU_T)}{1 + 0.5\,\exp((Vg - V_{T0})/NU_T)}. \quad (14)$$

η_{2f} is the asymptotic value of $\eta(Vg)$ at high gate voltages. N is a slope factor which minimizes the error between $\eta(Vg)$ and η_{21} in a large range $[N_A, t_{ox}]$. Under this condition $a(Vg)$ becomes

$$a(Vg)\,|_{V_D=0} = \frac{\exp\left(Q_{inv}(0)|_{Vg}/\eta(Vg) C_0 U_T\right) - 1}{\exp((Vg - V_T)/\eta_0 U_T)} \quad (15)$$

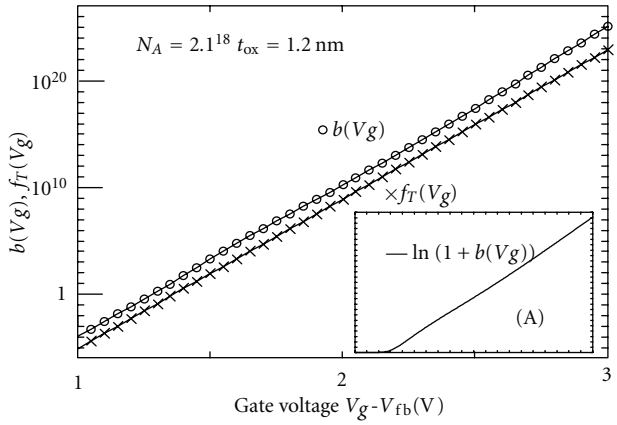

FIGURE 5: $b(Vg)$ from (18) (○○) and $f_T(Vg) = \exp(Vg - V_T/\eta_0 U_T)(\times\times)$. (A): $[\ln(1 + b(Vg)), Vg]$ plots.

with

$$Q_{\text{inv}}(0)|_{Vg} = Q_{\text{inv}}(V_D = 0)|_{Vg} = \lambda q n_i \int_0^{u_S(0)} \frac{e^u}{\sqrt{H(u) + G(u)}} du, \tag{16}$$

and $\widetilde{Q}_{\text{inv}}(Vg, V_D)$ is written as follows:

$$\widetilde{Q}_{\text{inv}\,0}(Vg, V_D) = \eta(Vg) C_0 U_T \ln\left[1 + b(Vg) \exp\left(-\frac{V_D}{U_T}\right)\right] \tag{17}$$

with

$$b(Vg) = a(Vg)\,|_{V_D=0} \exp\left(\frac{Vg - V_T}{\eta_0 U_T}\right) = \exp\left(\frac{Q_{\text{inv}}(0)|_{Vg}}{\eta(Vg) C_0 U_T}\right) - 1. \tag{18}$$

The coefficient $b(Vg)$ is dependent on the gate voltage Vg by $u_S(0)$ solution of (5) in $y = 0$. Equation (17) gives, respectively, in strong and weak inversion the simplified expressions:

$$\widetilde{Q}_{\text{inv}\,0}(Vg, V(y)) = Q_{\text{inv}}(0)|_{Vg} - \eta(Vg) C_0 V(y), \quad \widetilde{Q}_{\text{inv}\,0}(Vg, V(y)) = Q_{\text{inv}}(0)|_{Vg} \exp -\frac{V(y)}{U_T}. \tag{19}$$

$b(Vg)$ is a monotonic function in all inversion modes (Figure 5). The originality of the correction by $b(Vg)$ is to give an expression of the inversion charges $\widetilde{Q}_{\text{inv}\,0}(Vg, V_D)$ in which the threshold voltage is not explicit but included in $u_S(0)$ and appears in $[\ln(1 + b(Vg)), f(Vg)]$ plots.

The parameter $b(Vg)$ varies from 10^{25} to 10^{-5} and as shown in Figure 5 is different from $f_T(Vg) = \exp(Vg - V_T/\eta_0 U_T)$. Nevertheless, in usual applications (Section 7), the derivative $db(Vg)/dVg$ can be approximated by

$$\frac{db(Vg)}{dVg} = \frac{b(Vg)}{\eta_0 U_T}. \tag{20}$$

3.3. Equivalent Expression of Inversion Charge. By using the mathematical properties of the function:

$$f_2(x) = \frac{2\ln[1 + \exp(x/2)]}{1 + 2\exp(-x/2)} = \frac{2\exp(x/2)}{2 + \exp(x/2)} \ln\left[1 + \exp\left(\frac{x}{2}\right)\right] \tag{21}$$

which has some similarities with $f_1(x) = \ln[1 + \exp(x)]$ in the range $]-\infty, +\infty[$ then (17) can be rewritten by setting

$$X(Vg, V_D) = \sqrt{b(Vg)} \exp\left(-\frac{V_D}{2U_T}\right), \quad \Gamma(Vg) = \frac{1 + \sqrt{b(Vg)}}{1 + 0.5\sqrt{b(Vg)}}, \quad S(Vg) = \frac{1}{3} \exp\left(\frac{Vg - V_T}{\sigma}\right)^2, \tag{22}$$

$$\widetilde{Q}_{\text{inv}\,1}(Vg, V_D) = \eta(Vg) C_0 U_T \frac{\Gamma(Vg)}{1 - S(Vg)} \times \left\{\frac{X(Vg, V_D)}{1 + X(Vg, V_D)} \ln[1 + X(Vg, V_D)]\right\}. \tag{23}$$

(i) $\Gamma(Vg)$ is an adaptive factor which varies between 0.5 ($b(Vg) \gg 1$) and 1 ($b(Vg) \ll 1$);

(ii) $1 - S(Vg)$ and $\sigma^2 = 145$ are fitting factors which minimize the error between $\widetilde{Q}_{\text{inv}\,1}(Vg, V_D)$ and $\widetilde{Q}_{\text{inv}\,0}(Vg, V_D)$ at $b(Vg) = 1$.

These parameters are available in a large range of $[N_A, t_{ox}]$. Equation (23) gives an expression similar to the Unified MOSFET Channel Charge Model given by (7a) and (7b) in [10] and used in BSIM model [17]. Moreover, (17) and (23) are the synthesis between the expression of inversion charges given in [9, 10] in agreement with the theoretical model (11). Figure 6 shows the normalized expressions of the inversion charges $\widetilde{Q}_{\text{inv}\,(0,1)}(Vg, V_D)/\eta_0 C_0 U_T$ at $V(y) = 0$ as a function of the gate voltage.

The term in braces in (23) can be integrated versus V_D and gives an analytic expression of the drain current similar to Oguey and Cserveny model [7].

4. Analytic Model of the Drain Current

The general expression for the drain current $I_D(V_D)$ (including drift and diffusion) with a constant mobility μ_n follows:

$$I_D(V_D) = \mu_n \frac{W}{L} U_T \int_0^{\xi(L)} Q_{\text{inv}}(V(y))\,|_{Vg} d\xi. \tag{24}$$

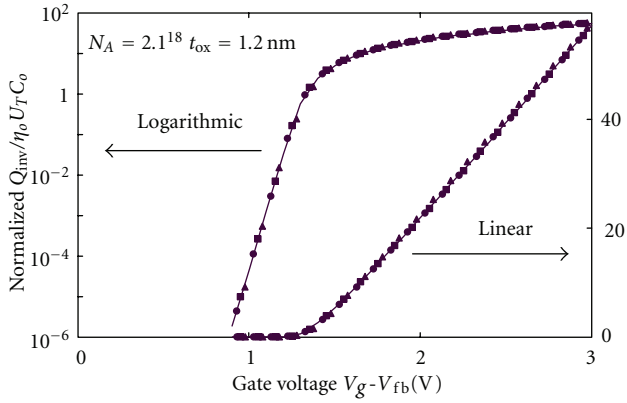

FIGURE 6: Normalized inversion charges $Q_{inv}(Vg, V_D = 0)\eta_0 C_0 U_T$ versus Vg in logarithm and linear scales. (−) (11), (■) (17), (•) (23), and (▲) (7a) and (7b) in [10].

4.1. The Pao-Sah Double Integral. Using the inversion charges dependence to drain bias $Q_{inv}(V(y))|_{Vg}$ (developed in Section 3.1), the Pao-Sah double integral then reads

$$I_{DPS}(V_D) = qn_i\mu_n \frac{W}{L} U_T^2 \int_0^{\xi(L)} \left\{ \int_{\xi(y)/2}^{u_S(y)} \frac{e^{u-\xi(y)}}{F(u,\xi(y))} du \right\} d\xi(y). \tag{25}$$

By substituting $d\xi(y)$ by $d\xi(y) = [d\xi(y)/du_S]du_S$, and grouping $e^{-\xi(y)}$ with $d\xi(y)/du_S$, the Pao-Sah double integral has no singular point and, (25) can be solved into iterated integrals from surface potential $u_S(y)$:

$$\begin{aligned} I_{DPS}(V_D) &= qn_i\mu_n \frac{W}{L} U_T^2 \int_{u_S(0)}^{u_S(L)} \left\{ \int_{\xi(y)/2}^{u_S} \frac{e^u}{F(u,\xi(y))} du \right\} \\ &\times \left[\frac{d}{du_S} \frac{G(u_S) - E(u_S)}{H(u_S)} \right] du_S. \end{aligned} \tag{26}$$

Equation (26) was previously calculated in a large range of drain and gate voltages and presented in [6].

4.2. Simplified Expression of the Drain Current. Equation (17) gives a simplified drain current expression in a single integral:

$$\begin{aligned} I_{\widetilde{Q}_{inv0}}(V_D) &= \mu_n \eta(Vg) C_0 U_T \frac{W}{L} \\ &\times \int_0^{V_D} \ln\left[1 + b(Vg) \exp\left(-\frac{V(y)}{U_T} \right) \right] dV(y). \end{aligned} \tag{27}$$

This expression describes the current-voltage characteristics in all inversion modes, insuring a continuous transition between weak and strong inversion. Unfortunately, there is no primitive function for the one defined by (27) which must be numerically calculated by classical integration methods.

4.3. Explicit Equation of the Drain Current. Following previous results we propose an analytic expression of the drain current in a square-logarithmic function of V_D based on the adaptive coefficient $b(Vg)$ by integration of (23).

$$\begin{aligned} I_{ap}\left(Vg, \frac{V_{DS}}{V_S}\right) &= I_{DA} \frac{\Gamma(Vg)}{1 - S(Vg)} \\ &\times \left\{ \ln^2[1 + X(Vg, V_S)] - \ln^2[1 + X(Vg, V_D)] \right\}, \end{aligned} \tag{28}$$

$$X\left(Vg, \frac{V_D}{V_S}\right) = \sqrt{b(Vg)} \exp\left(-\frac{V_D/V_S}{2U_T} \right), \tag{29}$$

$$I_{DA} = \mu_n \eta(Vg) C_0 U_T^2 \frac{W}{L}$$

is a dimensional factor.

The drain current, represented by a square-logarithmic function of gate and drain voltage, was proposed as early as 1982 by Oguey and Cserveny [7] in an analytic model based on a control voltage V_C derived from the gate voltage Vg and from drain source functions $f_w(V_D/V_S)$, $f_h(V_D/V_S)$:

$$\begin{aligned} I_{OC}(Vg, V_{DS}) &= \mu_n C_0 U_T^2 \frac{W}{L} [y(V_C, V_S) - y(V_C, V_D)], \\ y\left(V_C, \frac{V_D}{V_S}\right) &= \ln^2\left[1 + \exp f_w\left(\frac{V_D}{V_S}\right) + \exp f_h\left(\frac{V_D}{V_S}\right) \right]. \end{aligned} \tag{30}$$

The inversion charge of this model is given by

$$Q_{inv}|_{OcVg} = \frac{1}{\mu_n (W/L)} \frac{dI_{OC}(Vg, V_{DS})}{dV_D}. \tag{31}$$

Thereafter, the Oguey and Cserveny model has been simplified by Enz et al. [8]. The main difference in this paper is the use of the coefficient $b(Vg)$ instead of $f_T(Vg) = \exp(Vg - V_T/\eta_0 U_T)$.

Equations (27) and (28) (models 2 and 4) coincide with the double integral of Pao-Sah (model 1). The analytic models (Figure 7) are summarized in Table 1.

5. Mobility Model

In order to insure carrier drift velocity to be less than the saturation velocity v_{sat} at high electric field, a correction over constant mobility can be implemented in the drain current [18]. In the following, we use the mobility model developed by Roldan et al. [19]:

$$\mu_{neff} = \frac{\mu_1\left(\widetilde{F}_x\right)}{\left[1 + \left(\widetilde{F}_y / F_{sat} \right)^{\beta} \right]^{1/\beta}}. \tag{32}$$

5.1. Correction by the Transverse Electric Field F_x.

$$\mu_1\left(\widetilde{F}_x\right) = \frac{\mu_0}{\left[1 + \left(\widetilde{F}_x / F_0 \right) \right]}. \tag{33}$$

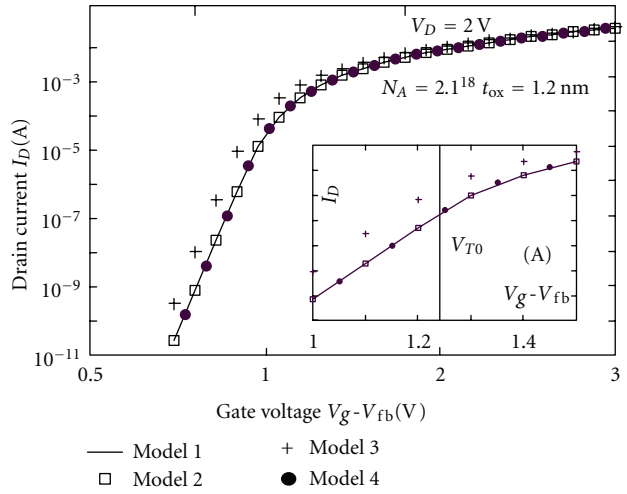

Figure 7: The different drain currents I_D versus Vg from models (1 − 4). (A): in the vicinity of the threshold voltage V_{T0}.

Table 1: Analytic models.

		Drain current	Inversion charges
Model 1	Pao-Sah integral	(25)	(11)
Model 2	Single integral	(27)	(13)
Model 3	[7]	(30)	(31)
Model 4	Analytic model	(28)	(23)

Several expressions are introduced to evaluate the mean electric field $\widetilde{F}_x$ in relation with the channel inversion charges. BSIM models introduce the voltage Vg_{steff} defined by (7a) and (7b) in [10]. An excellent approximation of Vg_{steff} can be obtained from the equivalent gate voltage Vg_{eff} defined from (17) as follows:

$$Vg_{\text{eff}} = \frac{\widetilde{Q}_{\text{inv}}(Vg, 0)}{C_0} = \eta(Vg)\, U_T \ln[1 + b(Vg)]. \tag{34}$$

The expression of the electric field calculated in (3) allows calculating $\widetilde{F}_x$ as the mean electric field in the inversion region with a dimensionless adaptive coefficient ua.

$$\widetilde{F}_x = \frac{ua}{2}\sqrt{\frac{2KTn_i}{\varepsilon_S}}\left(\sqrt{H\left[u_{S(y=0)}\right] + G\left[u_{S(y=0)}\right]} + \sqrt{H(0) + G(0)}\right). \tag{35}$$

Figure 8 shows the correction factors $\widetilde{F}_x$, compared with simplified BSIM 4.6.4 [17].

5.2. Correction by the Lateral Electric Field F_y. According to n-MOSFET models in [20, 21], we use $\beta = 2$:

$$\mu_{\text{neff}} = \frac{\mu_1\left(\widetilde{F}_x\right)}{\sqrt{1 + \left(\widetilde{F}_y/F_{\text{sat}}\right)^2}} \tag{36}$$

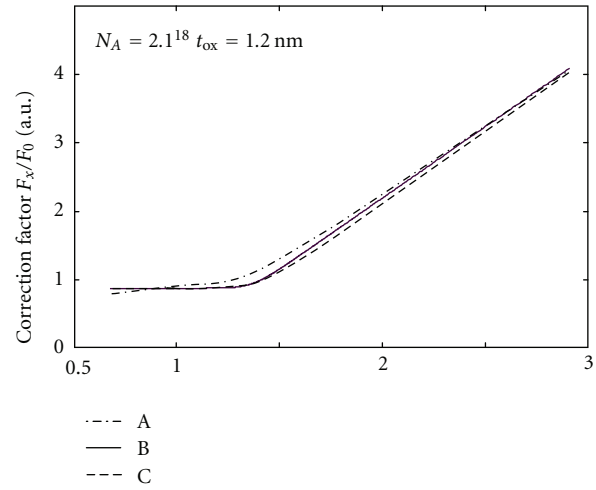

Figure 8: The correction factor F_x/F_0. (A) $(F_S(u_S(y)) + F_x(0))/2F_0$, (B) $Ua(Vg_{\text{steff}}+2V_{\text{th}})/t_{\text{ox}}$, and (C) $Ua(Vg_{\text{eff}}+2V\text{th})/t_{\text{ox}}$. ($F_0 = 0.67 \cdot 10^6 V \cdot \text{cm}^{-1}$.)

with

$$F_{\text{sat}} = \frac{\mu_1\left(\widetilde{F}_x\right)}{v_{\text{sat}}}, \tag{37}$$

and $\widetilde{F}_y$ the average of the lateral electric field:

$$\widetilde{F}_y = \frac{V_D}{L}. \tag{38}$$

The correction over constant mobility is introduced in the general expression of drain current by substituting μ_n by μ_{neff} in (24) as follows:

$$\mu_{n\text{eff}} = \frac{\mu_0}{\left[1 + \left(\widetilde{F}_x/F_0\right)\right]\sqrt{1 + \left\{\widetilde{F}_y v_{\text{sat}}\left[1 + \left(\widetilde{F}_x/F_0\right)\right]/\mu_0\right\}^2}}. \tag{39}$$

5.3. The Saturation Voltage V_{Dsat}. With mobility correction, the models of drain current $[I_{D,}V_D]$ present a maximum (Figure 9) at a saturation voltage V_{Dsat} defined, according to the mobility model by $I_{D,} = I_{D\,\text{sat}} = WQ_{\text{inv}}v_{\text{sat}}$ [17], $dI_D/d\Psi_S$ [20], or dI_D/dV_D [8]. $[I_{D,}V_D]$ curves are presented with the same model of correction by transverse electric field. The adaptive parameter in $\widetilde{F}_x$ must then be applied to give the same current and to minimize the error between measured and calculated data.

In this paper, $V_{D\,\text{sat}}$ represented on Figure 10 is calculated from the iterative definition of drain current (Section 4.1) with dI_D/dV_D substituted by $I_{D,m} - I_{D,m-1} = 0$. The saturation voltage is a linear function of Vg in strong inversion and becomes constant in weak inversion.

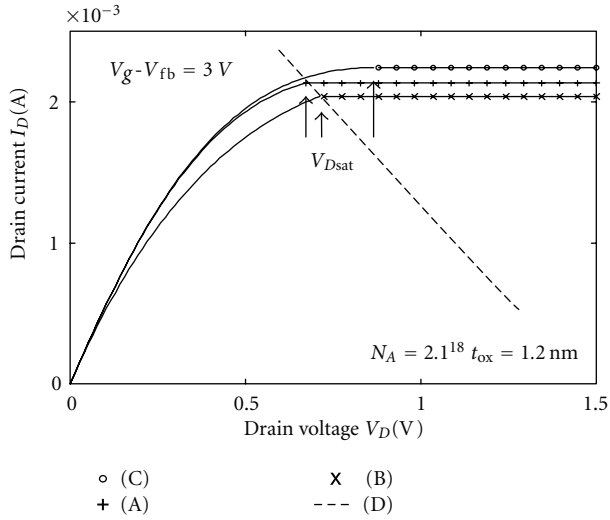

FIGURE 9: (I_D, V_D) plots with velocity saturation. (A) [17] ($\beta = 1$), (B) mobility correction with $\beta = 2$, (C) [20], and (D) saturation current $I_{D\,\mathrm{sat}} = WQ_{\mathrm{inv}}v_{\mathrm{sat}}$.

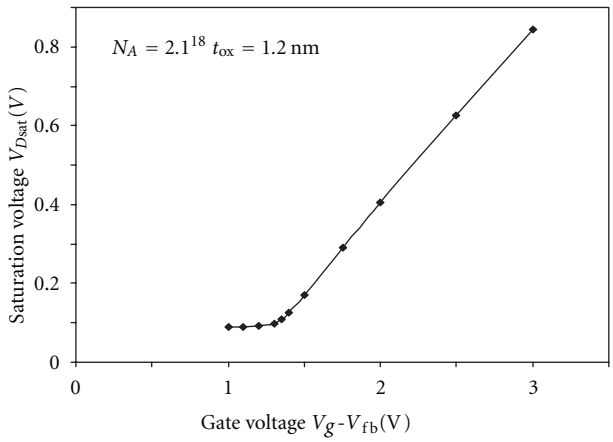

FIGURE 10: The saturation voltage $V_{D\,\mathrm{sat}}$ versus Vg. ($L = 90$ nm; $W/L = 10$.)

6. Short Channel Drain Current

6.1. Correction of Saturation Voltage. The drain current formulation with mobility μ_{neff} given from (39) is now written as follows:

$$I_D(V_D) = \mu_{n\mathrm{eff}}\frac{W}{L}U_T\int_0^{\xi(L)} \mathrm{Qinv}(V(y))\,|_{Vg}\,d\xi(y). \quad (40)$$

Equation (40) leads to an unphysical I_D, V_D, which must be clamped at $V_{D\,\mathrm{sat}}$. Gildenblat et al. [20] proposed to replace V_D by a smoothing function with a parameter ax : $V_{de} = V_D[1 + (V_D/V_{D\,\mathrm{sat}})^{ax}]^{-1/ax}$. From the analytical and explicit drain current expressions $I_{\tilde{Q}\mathrm{inv}\,0}(V_D)$ and $I_{\mathrm{ap}}(Vg, V_D)$, we can define a new function which includes

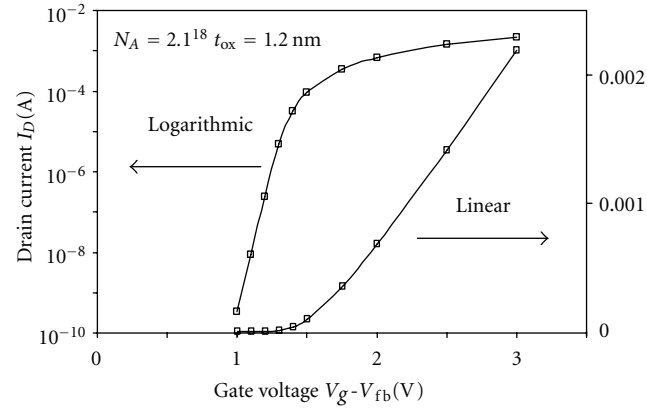

FIGURE 11: Transfer characteristics $I_{D11}(Vg)$ in logarithm and linear scales. $V_S = 0$; $V_D = 2$ V. ($L = 90$ nm; $W/L = 10$.)

the effect of velocity saturation by introducing the saturation voltage $V_{D\,\mathrm{sat}}$ in (27):

$$I_{D11}(V_D) = \frac{W}{L}\Gamma_1\eta_{21}C_0U_T \times \int_0^{V_D}\ln\left[1+\exp\left(\frac{V_{D\,\mathrm{sat}}-V(y)}{U_T}\right)\right]dV(y). \quad (41)$$

The coefficient Γ_1 fits $I_{D11}(V_D)$ with $I_{Q\mathrm{inv}}(V_D)$:

$$\Gamma_1 = \mu_{n\mathrm{eff}}(V_{D\,\mathrm{sat}}) \times \frac{\int_0^{V_{D\,\mathrm{sat}}}\ln[1+b(Vg)\exp(-V(y)/U_T)]dV(y)}{\int_0^{V_{D\,\mathrm{sat}}}\ln[1+\exp((V_{D\,\mathrm{sat}}-V(y))/U_T)]dV(y)} \quad (42)$$

and (28) becomes:

$$I_{D22}(V_{D\,\mathrm{sat}}, V_D) = \frac{W}{L}\Gamma_1\eta_{21}C_0U_T^2\frac{\Gamma(Vg)}{1-S(Vg)} \times \{Y_{02}^2(V_{D\,\mathrm{sat}}) - Y_{D2}^2(V_{D\,\mathrm{sat}}, V_D)\}, \quad (43)$$

$$Y_{02}(V_{D\,\mathrm{sat}}) = \ln\left[1+\exp\left(\frac{V_{D\,\mathrm{sat}}}{2U_T}\right)\right], \quad (44)$$

$$Y_{D2}(V_{D\,\mathrm{sat}}, V_D) = \ln\left[1+\exp\left(\frac{V_{D\,\mathrm{sat}}-V_D}{2U_T}\right)\right]. \quad (45)$$

6.2. Current-Voltage Characteristics. Figures 11 and 12 show the simulation results $[I_{D,}V_D]$ in strong and weak inversion with a mobility model deduced from (39).

The transfer characteristics $I_{D11}(Vg)$ (Figure 11) show linear variations in strong inversion and exponential variations in weak inversion. Figure 12 shows that the smoothing functions (41) and (43) give a unified formulation in the complete range of drain voltage.

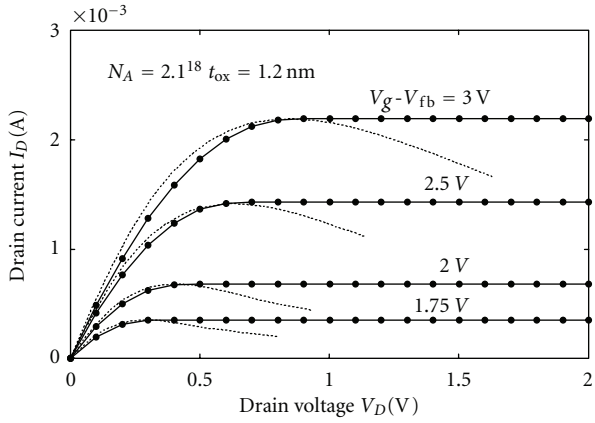

FIGURE 12: (I_D, V_D): (−) (41), (•) (43), (· · ·) (40). ($L = 90$ nm; $W/L = 10$.)

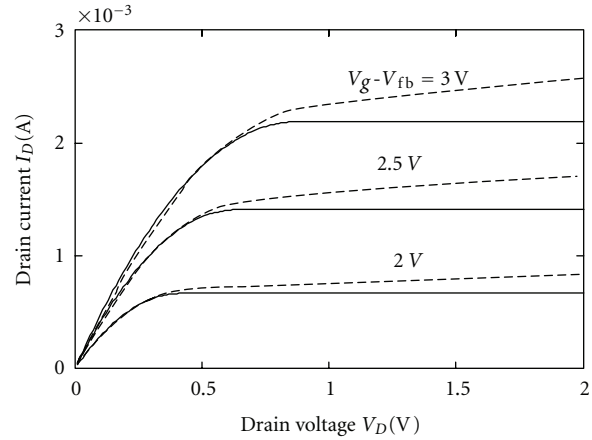

FIGURE 13: $I_D(V_D)$: (−) (43), (- -) (47). ($L = 90$ nm; $W/L = 10$.)

6.3. Channel Length Modulation. The channel length modulation (CLM) is a shortening of the length of the inverted channel region $L_{\text{eff}} = L - \Delta L$ due to inversion layer in the drain junction. An accurate calculation of ΔL requires solving the 2D Poisson equation near the drain. An 1D approach may be used for standard expression of the depletion layer in the abrupt junction approximation [22]

$$\Delta L = \sqrt{\frac{2\varepsilon_S}{qN_A}}\left[\sqrt{\frac{\varepsilon_S}{qN_A}\left(\frac{V_D}{L}\right)^2 + V_D} - \sqrt{\frac{\varepsilon_S}{qN_A}\left(\frac{V_D}{L}\right)^2}\right]. \tag{46}$$

Figure 13 shows an illustration of CLM with $I_D(V_D)$ from (41) modified by (46). The drain current formulation is

$$I_{\text{CLM}}(V_D) = \frac{L}{L - \Delta L} I_{D22}(V_D). \tag{47}$$

This approximation is analogous to the early voltage and has the advantage to be described by the single analytic function $I_{\text{CLM}}(V_D)$.

Figure 14 gives a complete summary of the different $I_D(V_D)$ as follows:

($\diamond$) are $I_D(V_D)$ data from Pao-Sah double integral from (40) with correction mobility in the range $0 < V_D < V_{D\,\text{sat}}$;

($\circ$) are $I_D(V_D)$ data from the saturation current corrected by the channel length modulation (46) ($V_{D\,\text{sat}} < V_D$);

(· · ·) are $I_{D11}(V_D)$ data from (41);

The full line shows the single analytic function $I_{\text{CLM}}(V_D)$ from (47).

6.4. Drain-Induced Barrier Lowering. The drain-induced barrier lowering (DIBL) was described as soon as 1979 by Troutman et al. [23]. The MOSFET is a three-terminal device in which source-channel drain is a $n - p - n$ (or $p - n - p$) double junction. We described in a previous paper the complete potential distribution in double junction from a 1D resolution of Poissons equation [24]. If this analytic description gives an accurate description of the potential $\varphi(x)$ in an unbiased double junction, the 1D resolution cannot be extrapolated with drain biased, which supposes a 2D device simulation. Most models describe the DIBL by a linear lowering of threshold voltage [21] $V_T = V_{T0} - \sigma V_D$ with the DIBL parameter σ.

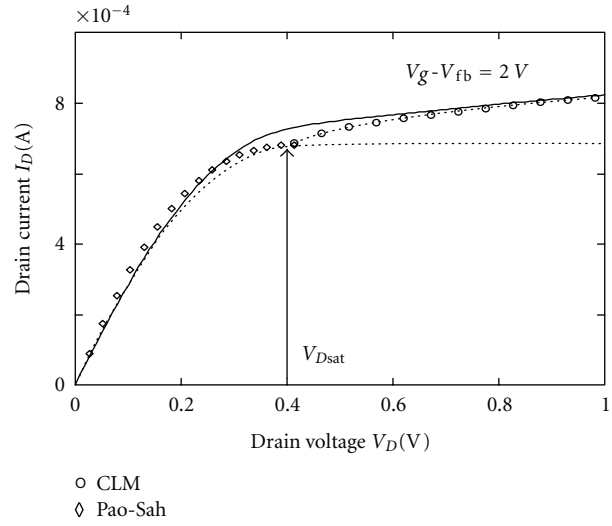

FIGURE 14: The different (I_D, V_D) plots with CLM. ($L = 90$ nm, $W/L = 10$.)

In this paper, following the model of DIBL in [25], we propose to insert the increase of inversion charge $\varepsilon_S dF_y(x, y)/dy$ by a quasi 1D calculation. With the same method, Cheng and Hu [26] calculated the threshold shift when $L \gg l = \sqrt{\varepsilon_S t_{ox} X_{dep}/\varepsilon_{ox}\kappa}$

$$\Delta V_{\text{th}} = [2(V_{bi} - 2\varphi_b) + V_D]\left[\exp\left(-\frac{L}{2l}\right) + 2\exp\left(-\frac{L}{l}\right)\right]. \tag{48}$$

In the present paper with $L = 90\,\text{nm}$, $L/l \approx 10$, ΔV_{th} is relatively a small correction in $I_D(V_D)$.

In [25], the authors propose, as shown on Figure 15, to add ΔV_{th} in the square logarithm with the new expressions:

$$Y_{02DB}(V_{D\,\text{sat}}) = \ln\left[1 + \exp\left(\frac{V_{D\,\text{sat}} + \Delta V_{\text{th}}(0)}{2U_T}\right)\right] \tag{49}$$

$$Y_{D2DB}(V_{D\,\text{sat}}, V_D) = \ln\left[1 + \exp\left(\frac{V_{D\,\text{sat}} - V_D + \Delta V_{\text{th}}(L)}{2U_T}\right)\right], \tag{50}$$

$$I_{\text{CLM+DIBL}}(V_D) = \frac{\Gamma(Vg)}{1 - S(Vg)} \frac{W}{L - \Delta L} \Gamma_1 \eta_{21} C_0 U_T^2 \times \{Y_{02DB}^2(V_{D\,\text{sat}}) - Y_{D2DB}^2(V_{D\,\text{sat}}, V_D)\}. \tag{51}$$

Due to the simplifying assumptions in the derivative $dF_y(x, y)/dy$, such a model gives a phenomenological description of DIBL, but must include fitting parameter to agree with experimental data. A new study is in progress in order to obtain a more accurate expression of $dF_y(x, y)/dy$ and apply this model to inversion charges in (41) and (43) taking into account the lateral field to provide a complete expression of DIBL.

In the case of n-MOSFETs, we have to add the Substrate Current-Induced Body Effect (SCIBE) which is the result of impact ionization by hot electrons coming from the source [23]. The expression of SCIBE is given by

$$I_{\text{sub}} = \frac{A}{B} I_D(V_D - V_{D\,\text{sat}}) \exp\left(-\frac{Bl}{V_D - V_{D\,\text{sat}}}\right). \tag{52}$$

A and B are adaptive parameters resulting from (I_D, V_D) measurements. In the present work, this effect must be added to (51) from A and B and gives the total current. Figure 16 shows an example of SCIBE with $L = 90\,\text{nm}$.

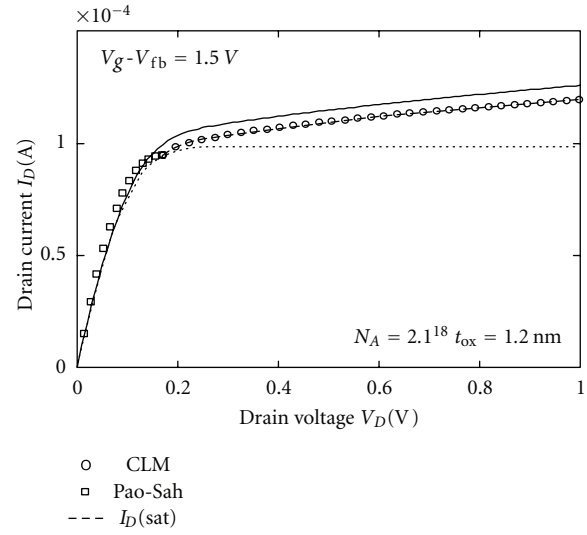

Figure 15: The total current $I_{\text{CLM+DIBL}}(V_D)$ $(-)$ from (51). ($L = 90\,\text{nm}$, $L/l = 9.5$, and $W/L = 10$).

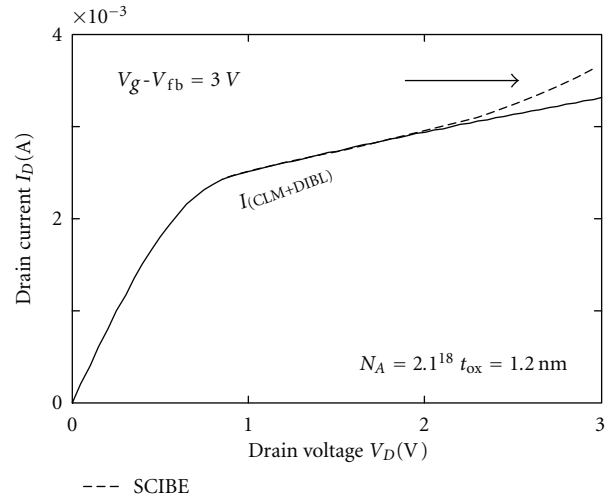

Figure 16: An example of SCIBE ($L = 90\,\text{nm}$; $W/L = 10$).

7. Analytic Model of TransConductance

The Pao-Sah double integral gives an expression of the transconductance from the derivative, $g = dI_D/dVg$ in (26) [6]:

$$g_{m\text{PS}} = qn_i\mu_{\text{neff}}U_T^2 \frac{W}{L} \times \int_{u_S(0)}^{u_S(L)} \frac{e^{u_S - \xi}}{F(u_S(y), \xi)} \left(\frac{du_S(y)}{dVg}\right) \left(\frac{d\xi(y)}{du_S(y)}\right) du_S(y). \tag{53}$$

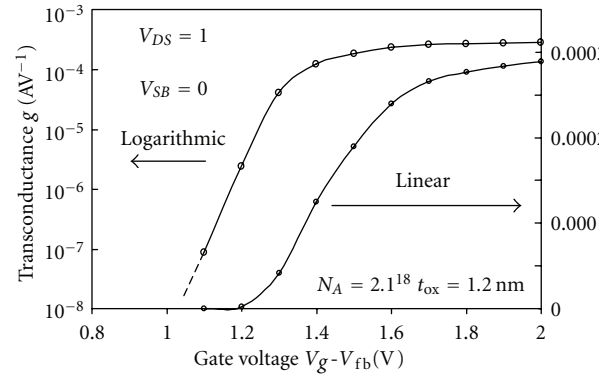

Figure 17: Transconductance versus Vg ($L = 90\,\text{nm}$; $W/L = 4$).

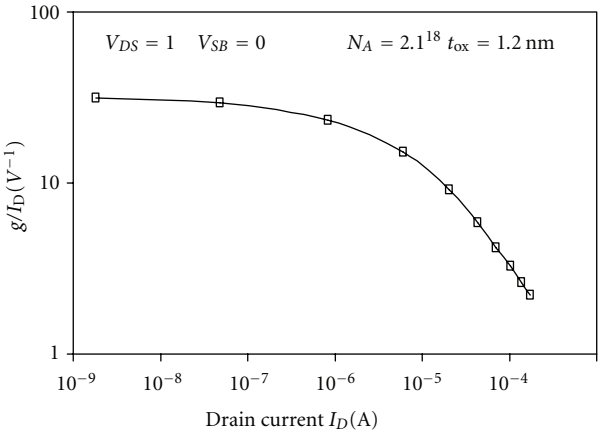

Figure 18: Normalized transconductance $[g/I_D, I_D]$. $V_{DS} = 1V$; $Vg - V_{fb} = 1{,}1.1, \ldots 2V$ ($L = 90$ nm; $W/L = 4$).

Table 2: The simplified analytic drain current models.

Physical constants	ε_S, ε_{ox}, KT/q
Process parameters	N_A, t_{ox}, μ_n, W/L
Device voltages	Vg, V_D, V_S, V_{fb}
Surface potential in $x = 0$, $y = 0$	$u_S(0)$
Surface potential	$u_S(y) = u_{S,m}$
Mobility	$\mu_{neff}(Vg, V_D)$
Drain current from Pao-sah	$I_{DPS}(V_D)$
Gate voltage factors	$\eta(V_g)$, $b(Vg)$
Analytic expression of drain current	$I_{ap}(Vg, V_D)$
Saturation voltage	$V_{D\,sat}$
Drain current with saturation	$I_{D22}(V_{D\,sat}, V_D)$
Channel length modulation	$I_{CLM}(V_D)$
Drain-induced barrier lowering	$I_{CLM+DIBL}(V_D)$

A simplified expression of the transconductance can be obtained from (27) by a derivative under the integral using $db(Vg)/dVg$ from (20) as follows:

$$g_{ma} = \left.\frac{dI_D}{dVg}\right|_{V_D} = \mu_{neff}\eta_{21}C_0U_T\frac{W}{L} \times \int_{V_S}^{V_D} \frac{(b(Vg)/\eta_0U_T)\exp(-V(y)/U_T)}{1 + b(Vg)\exp(-V(y)/U_T)}dV(y). \tag{54}$$

In this case, the integral in g_{ma} appears as $f'(v)/f(v)$, and g_{ma} is given by an analytical expression versus V_D and Vg:

$$g_{ma} = \mu_{neff}C_0U_T\frac{\eta_{21}}{\eta}\frac{W}{L}\ln\left\{\frac{1 + b(Vg)\exp(-V_S/U_T)}{1 + b(Vg)\exp(-V_D/U_T)}\right\}. \tag{55}$$

These expressions correspond to a long channel MOSFET with a constant mobility. The mobility model given by (39) introduces a second term in the transconductance due to Vertical Field Mobility Reduction (VFMR):

$$g_{m,\mu} = \frac{d\mu_{neff}}{dVg}\frac{I_D}{\mu_{neff}}. \tag{56}$$

$g_{m,\mu}$ is less than g_{ma} and appears as a corrective term in the transconductance. This contribution, negligible in long channel MOSFET, must be introduced as a corrective factor in the transconductance from

$$\frac{d\mu_{neff}}{dVg} = \frac{d\mu_{neff}}{d\mu_1}\frac{d\mu_1}{d\widetilde{F}_x}\frac{d\widetilde{F}_x}{du_S(0)}\frac{du_S(0)}{dVg}. \tag{57}$$

Each terms of this equation are calculated from (32), (33), (35), and (5). The contribution of CLM and DIBL in transconductance can be, respectively, deduced from (46), (47), (49), and (50).

A simple numerical calculation of the complete transconductance including VFMR, CLM, and DIBL is obtained from (51) by

$$g = \left.\frac{\Delta I_D}{\Delta V_g}\right|_{V_D}. \tag{58}$$

Figure 17 shows transconductance $[g, Vg]$ plots, and Figure 18 shows the "normalized" ratio $[g/I_D]$, versus drain current.

8. Conclusion

In this paper, we propose a solution of the Poisson-Boltzmann equation which describes the physical parameters of the MOSFET under gate and drain bias. The Taylor expansion of inverse functions is well suited in the case of implicit functions and gives an accurate solution of the channel potential $\xi(y) = f(u_S(y))$. We introduce an analytic function of the inversion charge giving an expression of the drain current insuring a continuous transition between weak and strong inversion associated with a simple expression of the transconductance. Furthermore, the method gives a good approach of drain current with the velocity saturation. All the equations have been solved with a simple C-encoding program available on all personal computers. This program, associated with a graphic user interface (Figure 19), generates a graph (Figure 20) with different Vg bias. The excellent agreement of the results obtained by an analytic continuous function of the inversion charge compared with those of standard models [1] can be considered as an accurate tool for microelectronics without access to specific CAD software and can provide a comprehensive overview of the complete MOSFET available in all inversion modes (Table 2).

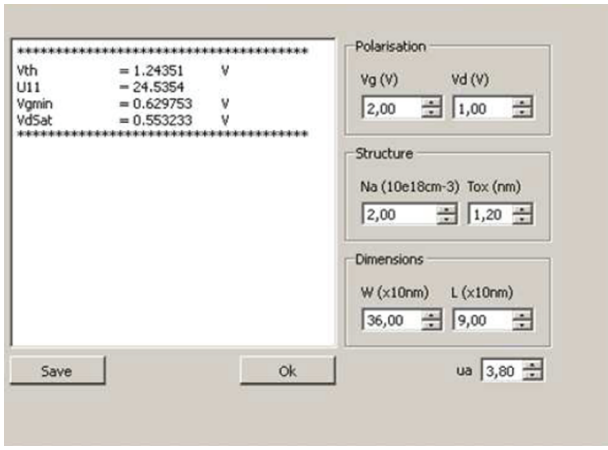

Figure 19: The graphic user interface.

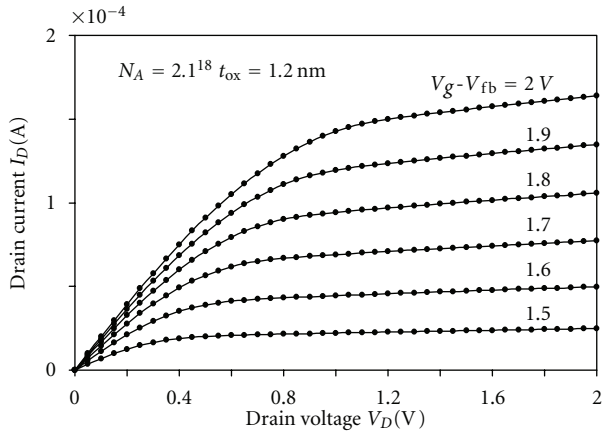

Figure 20: $I_D(V_D)$ plots from (51). $Vg - V_{fb} = 1.5, 1.6, \ldots 2V$.

Nomenclature

K and T: Boltzmann constant and temperature (Kelvin)
ε_S and ε_{ox}: silicon and silicon oxide permittivity
t_{ox}: oxide thickness
$C_0 = \varepsilon_{ox}/t_{ox}$: normalized oxide capacitance
$n_i = p_i$: intrinsic carrier concentration in cm^{-3}
N_A and N_D: dopant concentrations in cm^{-3}
$U_T = kT/q$: thermal voltage
$\varphi(b) = -U_T \ln(N_A/n_i)$: bulk potential of p-doped silicon
$u(x) = \varphi(x)/U_T$: reduced potential
$\Psi(x) = \varphi(x) - \varphi(b)$: band bending
$V_T = -2\varphi(b) + \sqrt{2qN_A\varepsilon_S|2\varphi(b)|}/C_0$: charge sheet threshold voltage
$\gamma_0 = \sqrt{2KT\varepsilon_S n_i}/C_0$: intrinsic body factor
$\lambda = \sqrt{KT\varepsilon_S/2q^2 n_i}$: Debye length (cm)
W, L: channel width and channel length.

Numerical applications use SI units, except for the following:

N_A, N_D, $n(x, y)$, and $p(x, y)$, in cm^{-3}.
inversion charges $Q_{\text{inv}}(Vg)|_{V(y)}$, $Q_{\text{inv}}(V(y))|_{Vg}$ in $\text{C}\cdot\text{cm}^{-2}$ and ε_S, ε_{ox} in $\text{farads}\cdot\text{cm}^{-1}$.

References

[1] J. Watts, C. M. Andrew, C. Enz et al., "Advanced compact models for MOSFETs," in *Proceedings of the Workshop on Compact Modeling at Nanotech*, pp. 3–12, Anaheim, Calif, USA, May 2005.

[2] R. Van Langevelde and F. M. Klaassen, "Explicit surface-potential-based MOSFET model for circuit simulation," *Solid-State Electronics*, vol. 44, no. 3, pp. 409–418, 2000.

[3] J. He, M. Chan, X. Zhang, and Y. Wang, "A physics-based analytic solution to the MOSFET surface potential from accumulation to strong-inversion region," *IEEE Transactions on Electron Devices*, vol. 53, no. 9, pp. 2008–2016, 2006.

[4] W. Z. Shangguan, M. Saeys, and X. Zhou, "Surface-potential solutions to the Pao-Sah voltage equation," *Solid-State Electronics*, vol. 50, no. 7-8, pp. 1320–1329, 2006.

[5] G. Gildenblat, Z. Zhu, and C. C. McAndrew, "Surface potential equation for bulk MOSFET," *Solid-State Electronics*, vol. 53, no. 1, pp. 11–13, 2009.

[6] H. Murray, P. Martin, and S. Bardy, "Taylor expansion of surface poten- tial in MOSFET: application to Pao-Sah integral," *Active and Passive Electronics Components*, vol. 2010, Article ID 268431, 11 pages, 2010.

[7] H. Oguey and S. Cserveny, "Modèle du transistor MOS valable dans un grand domaine de courants," *Bulletin SEV/VSE*, vol. 73, pp. 113–116, 1982.

[8] C. C. Enz, F. Krummenacher, and E. A. Vittoz, "An analytical MOS transistor model valid in all regions of operation and dedicated to low-voltage and low-current applications," *Analog Integrated Circuits and Signal Processing*, vol. 8, no. 1, pp. 83–114, 1995.

[9] B. Iniguez, L. F. Ferreira, B. Gentinne, and D. Flandre, "A physically-based C_∞-continuous fully-depleted SOI MOSFET model for analog applications," *IEEE Transactions on Electron Devices*, vol. 43, no. 4, pp. 568–574, 1996.

[10] Y. Cheng, K. Chen, K. Imai, and C. Hu, "A unified mosfet channel charge model for device modeling in circuit simulation," *IEEE Transactions on Computer-Aided Design of Integrated Circuits and Systems*, vol. 17, no. 8, pp. 641–644, 1998.

[11] C. K. Kim and E. S. Yang, ""On the validity of the gradual-channel approximation for field-effect transistors," *Proceedings of the IEEE*, vol. 58, no. 5, pp. 841–842, 1970.

[12] G. Goudet and C. Meuleau, *Semiconductors: Their Theory and Practice*, Macdonald & Evans, London, UK, 1957, English version by G. King.

[13] E. H. Nicollian and J. R. Brews, *MOS Physics and Technology*, John Wiley & Sons, Hoboken, NJ, USA, 2002.

[14] T. L. Chen and G. Gildenblat, "Analytical approximation for the MOSFET surface potential," *Solid-State Electronics*, vol. 45, no. 2, pp. 335–339, 2001.

[15] G. Baccarani, M. Rudan, and G. Spadini, ""Analytical i.g.f.e.t.model including drift and diffusion currents," *IEE Journal on Solid-State and Electron Devices*, vol. 2, no. 2, pp. 62–68, 1978.

[16] J. M. Sallese, M. Bucher, F. Krummenacher, and P. Fazan, "Inversion charge linearization in MOSFET modeling and rigorous derivation of the EKV compact model," *Solid-State Electronics*, vol. 47, no. 4, pp. 677–683, 2003.

[17] T. H. Morshed et al., "BSIM 4.6.4 MOSFET user manual," University of California, Berkeley, Calif, USA, 2009, http://www-device.eecs.berkeley.edu/bsim/Files/BSIM4/BSIM464/BSIM464_Manual.pdf.

[18] K. Y. Lim and X. Zhou, "Physically-based semi-empirical effective mobility model for MOSFET compact I-V modeling," *Solid-State Electronics*, vol. 45, no. 1, pp. 193–197, 2001.

[19] J. B. Roldan, F. Gamiz, J. A. Lopez-Villanueva, J. E. Carceller, and P. Cartujo, "The dependence of the electron mobility on the longit- udinal electric field in MOSFETs," *Semiconductor Science and Technology*, vol. 12, pp. 321–330, 1997.

[20] G. Gildenblat, X. Li, W. Wu et al., "PSP: an advanced surface-potential-based MOSFET model for circuit simulation," *IEEE Transactions on Electron Devices*, vol. 53, no. 9, pp. 1979–1993, 2006.

[21] N. Arora, *Mosfet Modeling for VLSI Simulation: Theory and Practice*, World Scientific Publishing, Singapore, 2007.

[22] J. J. Liou, A. Ortiz-Conde, and F. Garcia-Sanchez, *Analysis and Design of MOSFETs—Modeling, Simulation, and Parameter Extraction*, Kluwer Academic, Norwell, Mass, USA, 1998.

[23] S. C. Tam, F.-C. Hsu, P.-K. Ko, T.-Y. Chan, and K. W. Terrill, "Hot-electron induced MOSFET degradation—model, monitor, improvement," *IEEE Transactions on Electron Devices*, vol. 32, pp. 375–385, 1985.

[24] H. Murray, "Analytic resolution of Poisson-Boltzmann equation in nanometric semiconductor junctions," *Solid-State Electronics*, vol. 53, no. 1, pp. 107–116, 2009.

[25] C. C. Enz and E. A. Vittoz, *Charge Based MOS Transistor Modeling*, John Wiley & Sons, London, UK, 2006.

[26] Y. Cheng and C. Hu, *MOSFET Modeling & BSIM3 USer's Guide*, Kluwer Academic, New York, NY, USA, 2002.